Applied Physics Letters

Enhancement of spin–orbit torque via interfacial hydrogen and oxygen ion manipulation

Cite as: Appl. Phys. Lett. **115**, 092402 (2019); https://doi.org/10.1063/1.5110206
Submitted: 15 May 2019 . Accepted: 13 August 2019 . Published Online: 26 August 2019

W. L. Peng, J. Y. Zhang, G. N. Feng, X. L. Xu, C. Yang, Y. L. Jia, and G. H. Yu

Applied Physics Letters ARTICLE scitation.org/journal/apl

Enhancement of spin–orbit torque via interfacial hydrogen and oxygen ion manipulation

Cite as: Appl. Phys. Lett. **115**, 092402 (2019); doi: 10.1063/1.5110206
Submitted: 15 May 2019 · Accepted: 13 August 2019 ·
Published Online: 26 August 2019

W. L. Peng,[1,a] J. Y. Zhang,[1,a),b] G. N. Feng,[1] X. L. Xu,[1] C. Yang,[1] Y. L. Jia,[1] and G. H. Yu[1,2,b)]

AFFILIATIONS

[1]Department of Materials Physics and Chemistry, University of Science and Technology Beijing, Beijing 100083, China
[2]Beijing Laboratory of Metallic Materials and Processing for Modern Transportation, Beijing 100083, China

[a)]**Contributions:** W. L. Peng and J. Y. Zhang contributed equally to this work.
[b)]**Author to whom correspondence should be addressed:** jyzhang@ustb.edu.cn and ghyu@mater.ustb.edu.cn

ABSTRACT

We report a large enhancement of spin–orbit torque (SOT) in perpendicular Ta/CoFeB/MgO multilayers with interfacial H^+ and O^{2-} ion manipulations. By controlling both H^+ and O^{2-} ions at the CoFeB/MgO interface, the switching current density (J_c) is almost half of that for the single O^{2-} ion manipulated sample. Through harmonic measurements, we have found that both dampinglike effective field H_D and fieldlike effective field H_F are increased for the H^+ and O^{2-} ion manipulated samples. Interfacial structural results indicate that the H^+ and O^{2-} ion manipulations modulate the interfacial chemistry at the CoFeB/MgO interface, which suppresses the spin reflection and improves the spin absorption in the CoFeB layer. Our results can effectively improve the SOT and provide an effective way to modulate SOT.

Recently, due to its potential application in nonvolatile memories and logic devices, the magnetization reversal based on spin–orbit torque (SOT) in heavy metal (HM)/ferromagnet (FM)/oxide heterostructures has attracted great interest.[1–10] The pure spin-polarized current, which generated from an in-plane electric current due to the spin Hall effect (SHE)[11–13] or the Rashba effect,[14,15] transfers its angular momentum to the adjacent FM and enables the SOT on the magnetization, giving rise to magnetization switching,[16–18] domain wall motion,[19,20] and high-frequency oscillation.[21,22] With distinct differences from the conventional spin transfer torque (STT), the SOT-based spintronic devices have high stability, simplicity, and scalability.[23] However, the high switching current density J_c impedes its further development.[16,24,25] Among all research, the control of O^{2-} ion transport offers the most accessible means of SOT manipulation.[26,27] For example, Mishra *et al.* used the electric field to transport O^{2-} ions and modulate the HM/FM interfacial chemistry, which facilitates a reversible manipulation over the direction and magnitude of SOT.[28] Unfortunately, an electric field at the FM/oxide interface is small, owing to the Coulomb screening in the metal. Although an alternative approach known as voltage-control ionic liquid gating is larger, the ionic switching is inherently slower.[29,30] Therefore, O^{2-} ion transport by these means is difficult to induce an obvious manipulation of SOT. An available strategy to promote the O^{2-} transport is intensely required.

Alternatively, H^+, which is the smallest possible ion and relatively innocuous, has been an ideal replacer for inducing property changes without changing the chemical phase or the structure.[31,32] H^+ ions also have a strong reducibility which is much easier to integrate with O^{2-}. Most previous studies for SOT manipulation have focused mainly on the evolution and control of single ionic species. Increasing the number of transferrable ionic species to facilitate the ion transport for SOT manipulation has yet to be explored.

In this work, we report the SOT in the perpendicular Ta/CoFeB/MgO heterostructure with a different annealing condition. For the sample annealed in the wet N_2 atmosphere, the J_c has a large reduction, leading to the SOT switching efficiency (η) of 113% larger than that for the sample annealed in the vacuum. Considering the results of the interfacial structure analysis, for the sample annealed in the wet N_2 atmosphere, H_2O splitting reaction can be thermally catalyzed and then H^+ generated at the surface of the film is inserted into the CoFeB/MgO interface. The injected H^+ facilitates the O^{2-} migration from the CoFeB layer to the MgO layer. The effective H^+ and O^{2-} ion manipulations could directly improve the current-induced effective field, which not only improves the perpendicular magnetic anisotropy (PMA) but also effectively modulates the SOT.

Multilayers with the structure of Ta(5)/$Co_{40}Fe_{40}B_{20}$(1.1)/MgO(2)/Ta(1) (in nm) were deposited on thermally oxidized Si wafers at room temperature, using a magnetron sputtering system (AJA1800F). After film growth, Hall bars were fabricated by ultraviolet lithography and ion beam etching for transport measurements. Contact pads made of Cr(5 nm)/Au(65 nm) were additionally formed at each of the cross by

DC sputtering and lift-off technology. Thermal annealing was carried out at 250 °C for 30 min in the vacuum, the air, and the wet N_2 atmosphere (denoted as V, A, and W), respectively. The pressure of the thermal annealing in the vacuum was at 3×10^{-7} Torr. The N_2 gas (99.99% purity) flowed through de-ionized water to introduce H_2O into the chamber. The morphology of the Hall device can be investigated using scanning electron microscopy (SEM). The interfacial chemical states were characterized by the X-ray photoelectron spectroscopy system (XPS, ESCALAB 250Xi).

Figure 1(a) presents the structural schematic diagram of the samples along with the definition of the coordinate system. Figure 1(b) shows the SEM image of the Hall bar device with schematic illustrations of the measurement set-up, where the device channel width ω is 10 μm. Figure 1(c) shows Hall loops for samples annealed in V, A, and W. The square loops indicate a good PMA for three samples. Figure 1(d) shows the value of saturation magnetizations M_s and K_{eff} for samples annealed in V, A, and W. For the sample annealed in A, the value of K_{eff} is smaller than that of the sample annealed in V, indicating a decreased PMA. However, for the sample annealed in W, both M_s and K_{eff} are increased. Furthermore, the values of the effective anisotropy field H_{an} for samples annealed in V, A, and W are 7916 Oe, 7576 Oe, and 8919 Oe, respectively. The larger value of H_{an} for the sample annealed in W means a better PMA. It was demonstrated that the FM/oxide interface plays a significant role in PMA.[33,34] It indicates the changed interfacial state at the CoFeB/MgO interface for three samples. Figures 1(e) and 1(f) present the current-induced magnetization switching (CIMS) curves for three samples with in-plane field H_{ext} of ±50 Oe. The width of the pulse current is 100 μs, and the anomalous Hall resistance is measured after a 20-μs delay. With the in-plane field, the magnetization of CoFeB for three samples can be fully switched. Interestingly, the required J_c is quite different for three samples. The values of J_c for samples annealed in V, A, and W are 2.1×10^7 A/cm^2, 1.8×10^7 A/cm^2, and 1.1×10^7 A/cm^2, respectively. Figure 2(d) presents the SOT switching efficiency η [$\eta = (H_{an} - H_{ext})/J_c$] for three samples. It is found to be 3.8×10^2 Oe cm^2/MA, 4.2×10^2 Oe cm^2/MA, and 8.1×10^2 Oe cm^2/MA for samples annealed in V, A, and W, respectively. Compared with the sample annealed in V, the η for the sample annealed in A is merely increased by 11%, while that of the sample annealed in W is increased by 113%.

To further investigate the different SOT behavior, the harmonic measurements were conducted to evaluate the current-induced effective field. Two kinds of SOT, namely, dampinglike torque (DLT) and fieldlike torque (FLT), can be distinguished in Ta/CoFeB/MgO heterostructure, which is equivalently characterized by the H_D and H_F,[35–38]

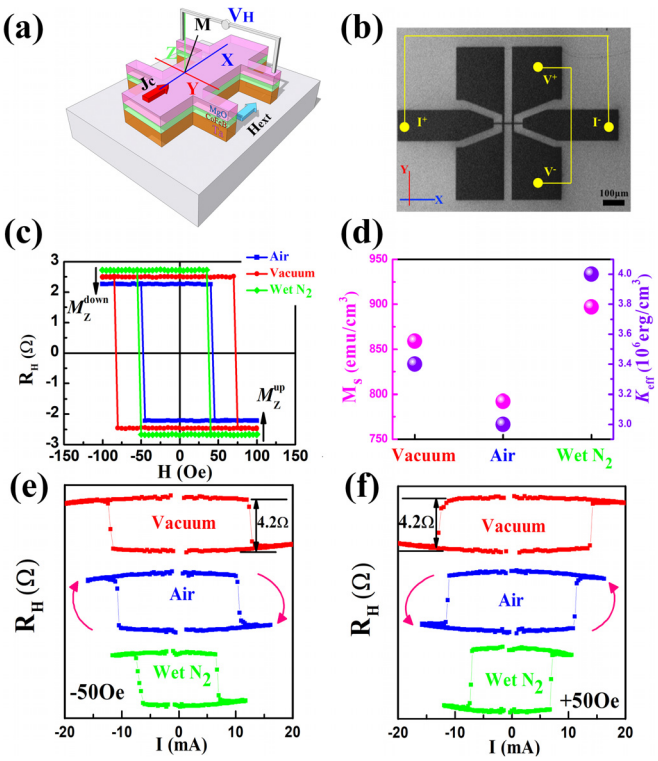

FIG. 1. (a) Structural schematic diagram of the Ta/CoFeB/MgO multilayers along with the definition of the coordinate system. (b) The micrograph of the Hall bar device with schematic illustrations of the measurements (scale bar 100 μm). (c) Hall loops for samples annealed in the vacuum (red), the air (blue), and the wet N_2 (green) atmosphere. (d) The value of the saturation magnetization M_s and effective magnetocrystalline energy K_{eff} for samples annealed in the vacuum, the air, and the wet N_2 atmosphere. (e) and (f) Current-induced magnetization switching curves with an in-plane field of ±50 Oe for samples annealed in the vacuum (red), the air (blue), and the wet N_2 (green) atmosphere.

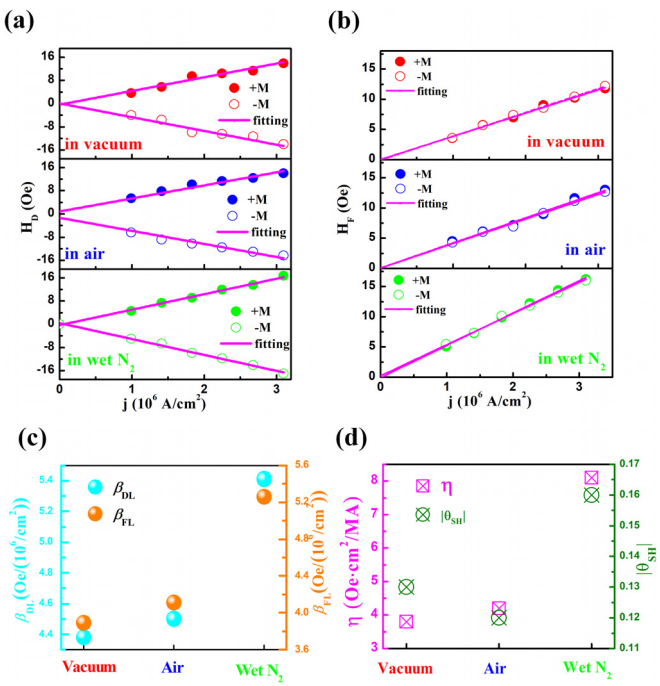

FIG. 2. (a) Dampinglike effective field H_D vs applied current density for samples annealed in the vacuum (red), the air (blue), and the wet N_2 (green) atmosphere. (b) Fieldlike effective field H_F vs applied current density for samples annealed in the vacuum (red), the air (blue), and the wet N_2 (green) atmosphere. (c) The strength of dampinglike effective field (β_{DL}) and fieldlike effective field (β_{FL}) for samples annealed in the vacuum, the air, and the wet N_2 atmosphere. (d) The values of spin–orbit torque switching efficiency η and the spin Hall angle θ_{SH} for samples annealed in the vacuum, the air, and the wet N_2 atmosphere.

respectively. A constant amplitude sinusoidal current with a frequency of 150 Hz was applied to the devices, which will exert a periodic SOT on the magnetization and induce magnetization oscillation around the equilibrium direction. The H_D and H_F for samples annealed in V, A, and W with the out-of-plane magnetization component $\pm M$ are calculated using the equations under the assumption that the planar Hall effect is smaller than the anomalous Hall effect,

$$\mu_0 H_{DL(FL)} = -2\mu_0 \frac{\partial V_{2\omega}}{\partial H_{x(Y)}} \Big/ \frac{\partial^2 V_\omega}{\partial H_{x(Y)}^2}. \quad (1)$$

They are plotted as a function of the current density j, as shown in Figs. 2(a) and 2(b), respectively. The current shunting percentages in the Ta underlayer and the CoFeB layer for three samples are almost the same, and thus we assume that the current densities in Ta for three samples were uniform throughout the Ta/CoFeB bilayers for the purpose of convenience. The $H_{D(F)}$ varies linearly with j, suggesting a negligible effect of Joule heating in the measured range. The slope of the fitted curves $\beta_{D(F)}$ can be expressed as the strength of DLT and FLT, respectively. The value of $\beta_{D(F)}$ is shown in Fig. 2(c). For the sample annealed in V, β_D and β_F are found to be 4.38 Oe/(10^6 A/cm^2) and 3.89 Oe/(10^6 A/cm^2), respectively. For the sample annealed in A, β_D and β_F are found to be 4.50 Oe/(10^6 A/cm^2) and 4.11 Oe/(10^6 A/cm^2), which is slightly increased by 3% and 6%, respectively. The change of DLT and FLT can be negligible. However, for the sample annealed in W, β_D and β_F are found to be 5.41 Oe/(10^6 A/cm^2) and 5.26 Oe/(10^6 A/cm^2), which is 24% and 35% larger than that of the sample annealed in V, respectively.

The interfacial state at the CoFeB/MgO interface was detected by XPS. Information about the electronic structure of the CoFeB/MgO interface can be obtained after an Ar^+ etching for 20s. More details about the XPS measurements can be found in our previous work.[39,40] Figure 3(a) shows the Fe $2p_{3/2}$ fitting curve high-resolution XPS spectra at the CoFeB/MgO interface for the as-deposited sample and samples annealed in V, A, and W, respectively. Although Fe oxide and Co oxide exist simultaneously at the interface, more attention should be paid to the Fe 2p XPS results because the intensity of Fe oxide is higher than that of Co oxide. From XPS handbook,[41] the peaks located at 713.3 eV for four samples correspond to a secondary Co transition auger peak, which will be discussed elsewhere. The peaks located at 707.0 eV, 707.8 eV, and 709.4 eV correspond to Fe $2p_{3/2}$ in metallic Fe, FeO_X(X < 1), and FeO, respectively. It indicates that metallic Fe at the CoFeB/MgO interface is partially oxidized for four samples. The relative Fe-O content at the interface can be estimated by the ratio of the peak area ($\varepsilon = S_{Fe}/S_{FeOx+FeO}$). The value of ε for four samples is shown in Fig. 3(c). The value of ε is 1.5 for the as-deposited sample. However, the value of ε is increased for samples with different annealing conditions. Fig. 3(b) presents the Mg 1s fitting curve high-resolution XPS spectra at the CoFeB/MgO interface for the as-deposited sample and samples annealed in V, A, and W, respectively. The binding energy χ of Mg 1s for four samples is shown in Fig. 3(c). Compared with the as-deposited sample, the peak of Mg 1s shifts 0.9 eV and 1.1 eV toward a higher binding energy for the sample annealed in V and A, respectively. However, the χ of Mg 1s for the sample annealed in W is 1303.4 eV, which shifts 0.8 eV toward a lower binding energy. From XPS handbook,[41] the χ of Mg 1s in $Mg(OH)_2$ is about 1302.7 eV, suggesting that the shift of Mg 1s for the sample annealed in W is ascribed to the generated $Mg(OH)_2$ at the CoFeB/MgO interface.

The XPS results suggest that different ion transports occurred at the CoFeB/MgO interface with different annealing conditions. For the as-deposited sample, the CoFeB layer is unavoidably oxidized during the deposition of the oxide capping layer.[42] The schematic diagram of the O^{2-} distribution for the as-deposited sample is shown in Fig. 4(a). For the sample annealed in V, the O^{2-} ion transport is thermally activated, leading to O^{2-} migration from the CoFeB layer to the MgO layer.[43,44] The schematic diagram of the O^{2-} migration for the sample annealed in V is shown in Fig. 4(b). It results in an increment of ε, which is 40% larger than that of the as-deposited sample. The peak of Mg 1s in MgO shifts toward a higher binding energy. Thus, only O^{2-}

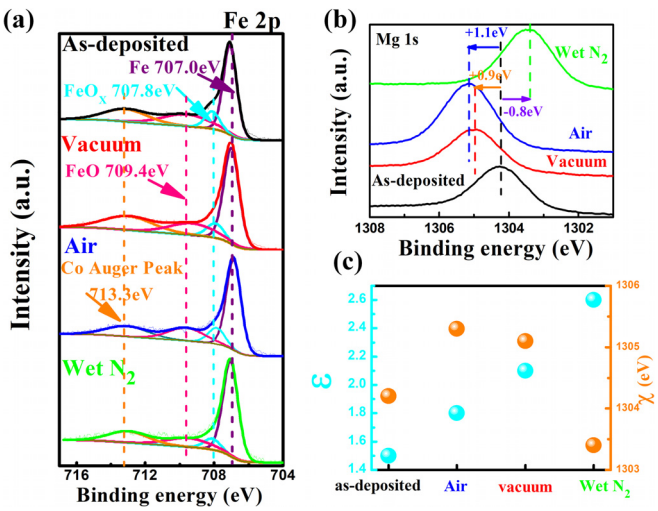

FIG. 3. (a) Fe 2p high-resolution XPS spectra for the as-deposited sample and samples annealed in the vacuum, the air, and the wet N_2 atmosphere. (b) Mg 1s high-resolution XPS spectra for the as-deposited sample and samples annealed in the vacuum, the air, and the wet N_2 atmosphere. (c) The relative Fe-O content ε and the binding energy χ of Mg 1s at the CoFeB/MgO interface for the as-deposited sample and samples annealed in the vacuum, the air, and the wet N_2 atmosphere.

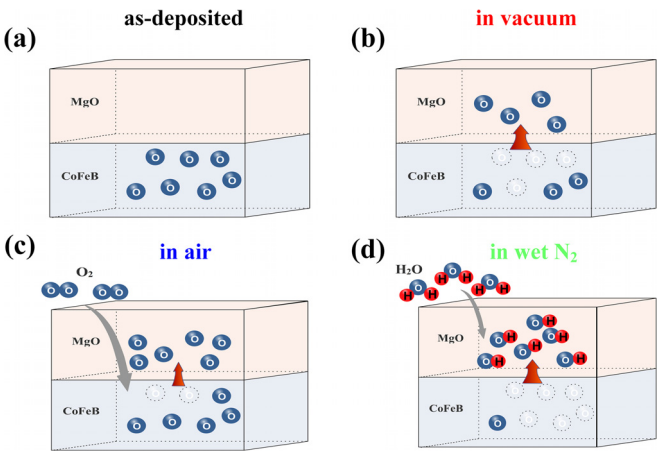

FIG. 4. Different O^{2-} distribution state and schematic diagram of ion transport at the CoFeB/MgO interface for (a) the as-deposited sample and samples annealed in (b) the vacuum, (c) the air, and (d) the wet N_2 atmosphere.

ion transport can be observed, and the chemical reaction at the CoFeB/MgO interface for the sample annealed in V can be expressed as

$$FeO + FeO_x(x < 1) + Mg \rightarrow Fe(medium) + MgO. \quad (2)$$

For the sample annealed in A, the CoFeB and the MgO layers are oxidized due to the O_2 in the air. The oxidation induced by the air and O^{2-} migration due to the thermal annealing have a joint effect on the interfacial chemistry. The ε has a slight increase, which is 20% larger than that of the as-deposited sample, and the peak of Mg 1s is a shift of 1.1 eV to a higher binding energy. Especially, by changing the annealing condition, the degree of O^{2-} migration can be suppressed. Since only the degree of O^{2-} migration engaged at the CoFeB/MgO interface changes, the chemical reaction at the interface for the sample annealed in A can be expressed as

$$FeO + FeO_x(x < 1) + Mg + O_2 \rightarrow Fe(little) + MgO. \quad (3)$$

For the sample annealed in W, it is proposed that H_2O is hydrolyzed at the surface of the film, producing H^+ and O^{2-} through the oxygen evolution reaction.[45] Thus, it is identified that H_2O in the wet N_2 atmosphere is the most likely origin of H^+. The inserted H^+ will capture O^{2-} which exists in the CoFeB/MgO to form $(OH)^{2-}$ because of its strong reducibility. For the sample annealed in V or A, a Mg^{2+} will combine with an O^{2-}. But for the sample annealed in W, a Mg^{2+} will interact with two O^{2-} due to the generated $Mg(OH)_2$. Therefore, the H^+ injection could promote the O^{2-} migration, giving rising to the H^+ and O^{2-} ion manipulations at the CoFeB/MgO interface. It is found to be a large increment of ε which is 73% larger than that of the as-deposited sample. The χ of Mg 1s shifts to 1303.4 eV. Thus, the chemical reaction at the CoFeB/MgO interface for the sample annealed in W can be expressed as

$$FeO + FeO_x(x < 1) + Mg + H^+ \rightarrow Fe(much) + Mg(OH)_2. \quad (4)$$

Compared with the sample annealed in V, the change of DLT and FLT can be negligible for the sample annealed in A, which suggests that single O^{2-} manipulation has almost no effect on the current-induced effective field. The degree of O^{2-} migration is too small to induce an obvious SOT manipulation. For the sample annealed in A, the decreased J_c is likely ascribed to the reduction of PMA.[25] However, for the sample annealed in W, the enhanced PMA could result in an increased J_c, which is unable to explain the variation. As the magnetization switching process is a thermally activated depinning process, the low coercive field could also result in a low J_c. Despite the coercive field for the sample annealed in A being almost the same as that for the sample annealed in W [shown in Fig. 1(c)], J_c is increased by 39%. It indicates that the variation of the coercive field is not the main reason for the different behaviors of SOT. For this to be the case, the origin of the different SOT behaviors is likely ascribed to the effective H^+ and O^{2-} ion manipulations induced by the changed ion transportation. Qiu *et al.* have found that the magnitude of SOT strongly depends on the amount of spin current absorbed in the FM.[46] Furthermore, they have also reported that the interfacial spin reflection of the FM/MgO interface is much larger than that of the FM/metal interface, which suppress the interfacial spin absorption. Assuming the DLT exerted on the magnetization arising from the spin current generated from the SHE of HM, the θ_{SH} of Ta can be estimated using the following equation:

$$H_D = \hbar\theta_{SH}|J|/(2|e|M_S t_F) \quad (5)$$

where t_F is the thickness of CoFeB. The value of θ_{SH} for three samples is shown in Fig. 2(d). It is found to be −0.13, −0.12, and −0.16 for samples annealed in V, A, and W, respectively. The value of θ_{SH} for the sample annealed in W is larger than that for samples annealed in V and A, indicating that the SHE-induced SOT is improved. For the sample annealed in V and A, the transverse spin currents from the Ta layer are not fully absorbed in FM due to the over-oxidized CoFeB. However, for the sample annealed in W, the oxidization of CoFeB is significantly decreased with the injection of H^+, which could facilitate the transverse spin current absorption. Furthermore, the injection of $H^{\pm}$ could effectively promote the O^{2-} migrated from the CoFeB layer back to the MgO layer, which could improve the interface properties and decrease the amount of interfacial spin scattering centers. It will promote the interfacial spin absorption by suppressing the reflection of the spin current at the CoFeB/MgO interface. These results effectively improve the transmitting of spin currents, which result in an enhancement of θ_{SH}. In addition, the broken inversion symmetry is also a source of SOT like the Rashba SOT. The strength of the Rashba SOT is sensitive to the spin–orbit coupling strength and the band structure, which, in turn, depend on the interfacial composition and quality.[47,48] Mishra *et al.* have found that the amount of current-induced spin accumulation at the HM/FM interface can be controlled using electric-field-induced oxygen migration at the FM/oxide interface.[28] The O^{2-} ion transport manipulates the interfacial chemistry, leading to the interplay between the spin Hall and interfacial Rashba SOT. In our work, the injection of H^+ could also modify the distribution of O^{2-} in the CoFeB layer, which reduces the oxidization of the Ta/CoFeB interface. Hence, the magnitude of the interfacial Rashba SOT keeps increasing. The improved SHE-induced SOT and interfacial Rashba SOT could, in turn, exert more torques on the magnetization of CoFeB, inducing the large increment of SOT. On the other hand, the Dzyaloshinskii-Moriya interaction (DMI) also plays an important role in the SOT-induced magnetization switching. The SOT is found to originate mostly from the bulk of an HM, while DMI is more of an interfacial origin. The changed oxidization of the Ta/CoFeB interface induced by the injection of $H^{\pm}$ could also result in a changed interfacial DMI, which will affect the SOT. Thus, there is still much room for further experimental works toward $H^{\pm}$-based SOT manipulation.

In summary, the SOT in perpendicular Ta/CoFeB/MgO heterostructure with different interfacial ion manipulations was systematically investigated. The injection of H^+ at the CoFeB/MgO interface increases the number of transportable ionic species. The interfacial H^+ and O^{2-} ion manipulations effectively reduce the oxidization of the CoFeB layer, which contributes to the spin current absorption. It also modulates the interfacial chemistry, which suppress the spin reflection. The SHE-induced SOT can be effectively enhanced. On the other hand, the changed distribution state of O^{2-} in the CoFeB layer also contributes to the interfacial Rashba SOT. Therefore, both DLT and FLT have been increased for the H^+ and O^{2-} ion manipulated samples, which result in a large enhancement of SOT efficiency. The effective interfacial H^+ and O^{2-} ion manipulations not only improve the PMA in CoFeB layer but also modulate the SOT.

This work was supported by the National Key R&D Program of China (Grant No. 2017YFB0305502-01), the Natural Science Foundation of China (Grant Nos. 51571017, 51871018, and

11874082), and the National Key Scientific Research Projects of China Grant No. 2015CB921502.

REFERENCES

[1]S. A. Wolf, D. D. Awschalom, R. A. Buhrman, J. M. Daughton, S. V. Molnar, M. L. Roukes, A. Y. Chtchelkanova, and D. M. Treger, Science **294**, 1488 (2001).
[2]I. Zutic, J. Fabian, and S. D. Sarma, Rev. Mod. Phys. **76**, 323 (2004).
[3]D. D. Awschalom and M. E. Flatte, Nat. Phys. **3**, 153 (2007).
[4]T. P. Pareek, Phys. Rev. B **75**, 115308 (2007).
[5]A. Manchon and S. Zhang, Phys. Rev. B **78**, 212405 (2008).
[6]P. M. Haney and M. D. Stiles, Phys. Rev. Lett. **105**, 126602 (2010).
[7]L. Q. Liu, T. Moriyama, D. C. Ralph, and R. A. Buhrman, Phys. Rev. Lett. **106**, 036601 (2011).
[8]L. Q. Liu, C. F. Pai, Y. Li, H. W. Tseng, D. C. Ralph, and R. A. Buhrman, Science **336**, 555 (2012).
[9]L. Q. Liu, O. J. Lee, T. J. Gudmundsen, D. C. Ralph, and R. A. Buhrman, Phys. Rev. Lett. **109**, 096602 (2012).
[10]A. Brataas, A. D. Kent, and H. Ohno, Nat. Mater. **11**, 372 (2012).
[11]M. I. Dyakonov and V. I. Perel, Phys. Lett. A **35**, 459 (1971).
[12]J. E. Hirsch, Phys. Rev. Lett. **83**, 1834 (1999).
[13]T. Jungwirth, J. Wunderlich, and K. Olejnk, Nat. Mater. **11**, 382 (2012).
[14]V. M. Edelstein, Solid State Commun. **73**, 233 (1990).
[15]A. Manchon and S. Zhang, Phys. Rev. B **79**, 094422 (2009).
[16]S. Fukami, T. Anekawa, C. Zhang, and H. Ohno, Nat. Nanotechnol. **11**, 621 (2016).
[17]P. Li, T. Liu, H. Chang, A. Kalitsov, W. Zhang, G. Csaba, W. Li, and M. Wu, Nat. Commun. **7**, 12688 (2016).
[18]G. Y. Shi, C. H. Wan, Y. S. Chang, F. Li, X. J. Zhou, P. X. Zhang, J. W. Cai, X. F. Han, F. Pan, and C. Song, Phys. Rev. B **95**, 104435 (2017).
[19]S. Emori, U. Bauer, S. M. Ahn, E. Martinez, and G. S. D. Beach, Nat. Mater. **12**, 611 (2013).
[20]C. K. Safeer, E. Jue, A. Lopez, L. Buda-Prejbeanu, S. Auffret, S. Pizzini, O. Boulle, and I. M. Miron, Nat. Nanotechnol. **11**, 143 (2016).
[21]H. Mazraati, S. Chung, A. Houshang, and J. Akerman, Appl. Phys. Lett. **109**, 242402 (2016).
[22]O. Johansen and J. Linder, Sci. Rep. **6**, 33845 (2016).
[23]X. P. Qiu, Z. Shi, W. J. Fan, S. M. Zhou, and H. Yang, Adv. Mater. **30**, 1705699 (2018).
[24]J. Y. Chen, M. DC, D. L. Zhang, Z. Y. Zhao, M. Li, and J. P. Wang, Appl. Phys. Lett. **111**, 012402 (2017).
[25]X. Chen, Y. Liu, G. Yang, H. Shi, C. Hu, M. H. Liu, and H. B. Zeng, Nat. Commun. **9**, 2569 (2018).
[26]K. U. Demasius, T. Phung, W. F. Zhang, and S. S. P. Parkin, Nat. Commun. **7**, 10644 (2016).
[27]X. P. Qiu, K. Narayanapillai, Y. Wu, and H. Yang, Nat. Nanotechnol. **10**, 333 (2015).
[28]R. Mishra, F. Mahfouzi, D. Kumar, X. P. Qiu, and H. Yang, Nat. Commun. **10**, 248 (2019).
[29]U. Bauer, Nat. Mater. **14**, 174 (2014).
[30]C. Bi, Phys. Rev. Lett. **113**, 267202 (2014).
[31]A. J. Tan, M. Huang, C. O. Avci, and G. S. D. Beach, Nat. Mater. **18**, 35 (2019).
[32]D. A. Gilbert, A. J. Grutter, E. Arenholz, K. Liu, and B. B. Maranville, Nat. Commun. **7**, 12264 (2016).
[33]C. H. Lambert, A. Rajanikanth, T. Hauuet, E. E. Fullerton, and S. Andrieu, Appl. Phys. Lett. **102**, 122410 (2013).
[34]S. Nazir, S. Jiang, J. L. Cheng, and K. Yang, Appl. Phys. Lett. **114**, 072407 (2019).
[35]C. F. Pai, L. Liu, Y. Li, H. W. Tseng, D. C. Ralph, and R. A. Buhrman, Appl. Phys. Lett. **101**, 122404 (2012).
[36]U. H. Pi, Appl. Phys. Lett. **97**, 162507 (2010).
[37]M. Jamali, K. Narayanapillai, X. P. Qiu, and H. Yang, Phys. Rev. Lett. **111**, 246602 (2013).
[38]M. Hayashi, J. Kim, M. Yamanouchi, and H. Ohno, Phys. Rev. B **89**, 144425 (2014).
[39]J. Y. Zhang, Q. Y. Sun, Y. W. Liu, W. L. Peng, F. M. Wang, Y. D. Pan, L. Ding, and G. H. Yu, Appl. Surf. Sci. **396**, 1667 (2017).
[40]J. Y. Zhang, W. L. Peng, Q. Y. Sun, Y. W. Liu, B. W. Dong, X. Q. Zheng, G. H. Yu, C. Wang, Y. C. Zhao, and S. G. Wang, Appl. Surf. Sci. **436**, 22 (2018).
[41]C. D. Wanger, W. M. Riggs, L. E. Davis, J. F. Moulder, and G. E. Muilenberg, *Handbook of X-ray Photoelectron Spectroscopy* (Handbook of X-Ray Photoelectron Spectroscopy, 1970), Vol. p, p. 190.
[42]W. L. Peng, J. Y. Zhang, L. S. Luo, G. N. Feng, and G. H. Yu, J. Appl. Phys. **125**, 093906 (2019).
[43]X. Chen, C. Feng, Z. L. Wu, F. Yang, Y. Liu, S. Jiang, M. H. Liu, and G. H. Yu, Appl. Phys. Lett. **104**, 052413 (2014).
[44]X. Chen, K. Y. Wang, Z. L. Wu, S. L. Jiang, G. Yang, Y. Liu, J. Teng, and G. H. Yu, Appl. Phys. Lett. **105**, 092402 (2014).
[45]J. Rossmeisl, A. Logadottir, and J. K. Norskov, Chem. Phys. **319**, 178 (2005).
[46]X. P. Qiu, W. Legrand, P. He, Y. Wu, J. W. Yu, R. Ramaswamy, A. Manchon, and H. Yang, Phys. Rev. Lett. **117**, 217206 (2016).
[47]O. Krupin, Phys. Rev. B **71**, 201403 (2005).
[48]J. H. Park, C. H. Kim, H. W. Lee, and J. H. Han, Phys. Rev. B **87**, 041301 (2013).